Real-time Optical Monitoring of Ammonia Flow and Decomposition Kinetics under High-Pressure Chemical Vapor Deposition Conditions

Nikolaus Dietz∗, Martin Straßburg and Vincent Woods

Georgia State University, Department of Physics and Astronomy, Atlanta, Georgia USA

Abstract

Understanding the gas phase decomposition kinetics of the chemical precursors involved in the nucleation and thin film growth processes is crucial for controlling the surface kinetics and the growth process. The growth of emerging materials such as InN and related alloys requires deposition methods operating at elevated vapor densities due to the high thermal decomposition pressure in these materials. High nitrogen over-pressure has been demonstrated to suppress the thermal decomposition of InN, but has so far not been explored in chemical vapor deposition experiments. In this contribution we present research results on the decomposition kinetics of ammonia in the laminar flow regime of a high-pressure flow channel reactor. Ultraviolet absorption spectroscopy (UVAS) is applied to analyze absorption features of ammonia with respect to the ammonia flow rate during continuous flow and pulsed ammonia injection. Pulsed ammonia injection has been used to analyze the average gas flow velocity in the high pressure chemical vapor deposition (HPCVD) system as function of the total gas flow rate and the reactor pressure. The onset of the kinetics related to the decomposition of ammonia was found to start above 900K and showed a marked decrease for higher reactor pressures, thus decreasing the discrepancy of trimethylindium and ammonia decomposition temperatures.

∗ Electronic mail: ndietz@gsu.edu

I. Introduction

Improvements in the materials quality and a more detailed understanding of the growth kinetics of group III-nitride compound semiconductors is of crucial importance to advance the fabrication of optical electronic device structures. Even though much progress has been made for the GaN material system, InN and AlN have become increasingly significant due to their unique properties as low band gap and wide band gap material, respectively. At present, low-pressure deposition processes such as organometallic chemical vapor deposition (OMCVD - also denoted as MOVPE)[1,2] and molecular beam epitaxy (MBE)[3,4] are used, with limitations in the temperature regime and the control of the partial pressures of the constituents. The off-equilibrium conditions employed in MBE and OMCVD for the growth of InN also require low growth temperatures to overcome the thermal decomposition pressures, thus limiting the quality of InN and related group III-nitride epilayers[5-8], as outlined in controversial reviews on the present status of InN growth and characterization provided by Bhuiyan et al.[8] and Davydov et al.[9].

In order to get a handle on the vast difference in the vapor particle pressures of group III elements and nitrogen, and to control the thermal decomposition pressures over the growth surface, new approaches for the growth of In-rich group-III-nitride alloys need to be explored to control the point defect chemistry, leading to improved structural and optical properties of InN and related alloys.

Recent studies of the indium - nitrogen system[10] show much uncertainty in the p - T - x relationship due to missing experimental validation. However, studies of the nitrogen pressure required to prevent thermal decomposition of bulk InN, provided a relationship given by

$$p(N_2) \rightarrow p_0 \exp\left[-\frac{\Delta H_r}{R} \left(\frac{1}{T} - \frac{1}{T_0} \right) \right] , \qquad (1)$$

which results in the p-T^{-1} relation shown in Figure 1[11]. The relation indicates that in the pressure range $p_{N_2} \leq 10^2$ bar and for substrate temperatures ≤ 900 K the surface decomposition of InN will be effectively suppressed.

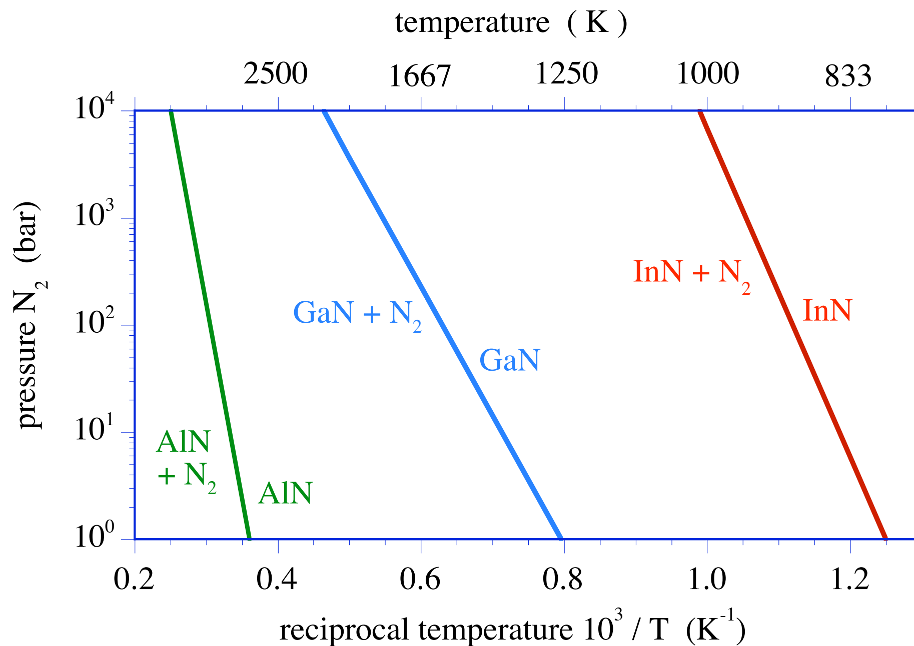

Figure 1:

Thermal decomposition pressure vs. reciprocal temperature for AlN, GaN and InN. Values are taken from ref.[11].

The here presented research focuses on the growth of group III-nitrides under high pressure chemical vapor deposition (HPCVD) conditions using InN as a model system in order to demonstrate the capabilities of HPCVD. InN is the most challenging material system, due to the fact that the equilibrium vapor pressure of nitrogen over InN is much higher as compared to AlN and GaN[12]. A high-pressure flow channel reactor with incorporated real time optical characterization capabilities[13-17] is utilized to study and optimize the InN nucleation and growth[18-21]. At above atmospheric pressures, optical diagnostic techniques are uniquely suited to provide real time information pertaining to gas flow dynamics in the laminar and turbulent flow regimes. Optical diagnostics are also being utilized to obtain crucial information on the precursor flow and decomposition kinetics. Several optical techniques have been explored, but only a small group satisfy the requirements of being robust as well as sensitive. For example, the substrate temperature during typical InN growth lays between 800K and 1200K, emitting significant visible and infrared radiation[17]. This favors the utilization of ultraviolet absorption spectroscopy (UVAS) or ultraviolet induced fluorescence spectroscopy to identify the group-V and organometallic group-III precursors in the gas phase, a technique well established in literature[22-25].

Moving towards HPCVD for the growth of group III-nitrides requires a reactor design with additional considerations towards flow kinetics, gas phase reactions, diffusion through the surface boundary layer as well as altered surface chemistry[26]. To *minimize* gas phase reactions, extract sufficient organometallic (OM) nutrients from the bubbler, and embed the precursor flow in the main reactor gas stream, a pulsed precursor injection scheme has been implemented, which is essential for

- *compression of precursors to reactor pressure,*
- *minimization of gas phase reactions,*
- *engineered nucleation kinetics and layer growth, and*
- *analyzing the gas-phase and surface decomposition dynamics in real-time.*

The implementation of the HPCVD system is schematically depicted in Figure 2, which shows the reactor cross section containing the substrates and optical monitoring plane, perpendicular to the flow direction. The flow channel is embedded in an inner reactor cylinder, while an outer reactor pressure vessel confines the overall pressure for well above 100 bar. The substrates are symmetrically embedded in the upper and lower part of the flow channel in order to prevent preferential material deposition. Optical access ports are integrated along the center axis of the substrates, allowing optical characterization of flow kinetics, gas phase reactions via laser light scattering (LLS) and UVAS. The optical access ports provide also access to the substrate surface through the back side, enabling the use of principal angle reflectance spectroscopy (PARS) and LLS in back-scattering geometry[13,17,27].

The HPCVD flow characteristics were analyzed using laser light scattering (LLS) in a forward scattering geometry[15,16], indicating that laminar flow conditions can be maintained in the flow and pressure regime of 1 standard liter per min (slm) to 16 slm and 1 bar to 15 bar, respectively.

The associated Reynolds number of the reactor flow channel averaged around 1480 with no significant pressure dependency observed[17].

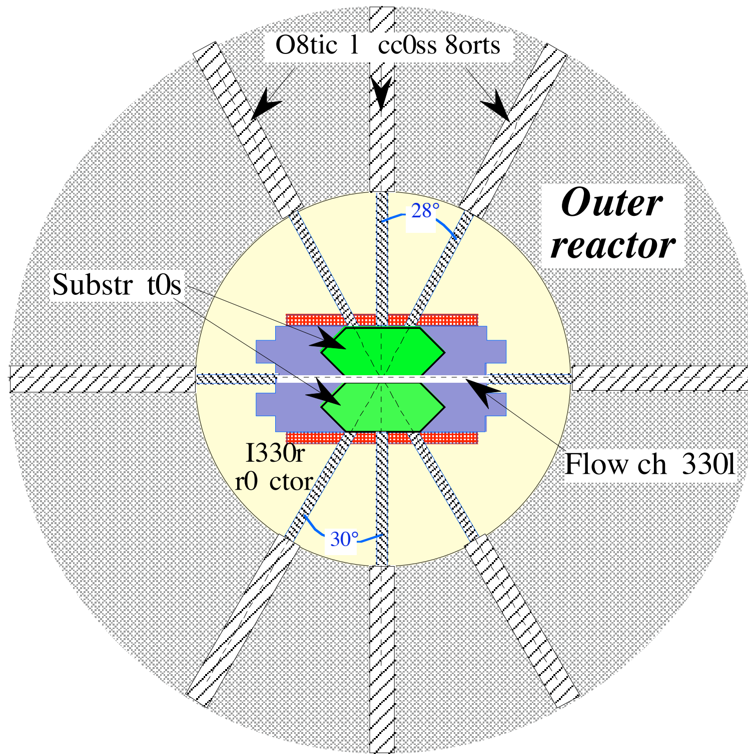

Figure 2:

Schematic cross section of the reactor containing the optical access ports and the center of the substrates. Two optical ports provide access to the flow channel and three ports in each of the two half sections of the reactor provide access to the growth surface.

In the following sections, we present the optical characterization of ammonia during continuous and pulsed injection. As outlined above, the pulsed precursor injection scheme is primarily essential for the compression of precursors up to reactor pressures. However, it is also crucial for analyzing and controlling the gas-phase and surface decomposition dynamics.

II. UVAS characterization of continuous ammonia flow

The optical characterization of NH_3 is treated separately for continuous flow and pulsed NH_3 injection. Under continuous flow condition, the vapor is transported from a gas cylinder, with a pressure set at 30 psi. The NH_3 flow is controlled via a mass flow controller with a 1 slm maximum flow, expressed via y = 1 -100% full scale (FS). The molar flow of ammonia and number of ammonia molecules per unit time are given by

$$n_{NH_3} = 7.4405\ 10^{-6}\ y\ \ [mol\ s^{-1}] \text{ and } N_{NH_3} = 4.4808 \cdot 10^{18} \cdot y\ \ [s^{-1}],\ \ (y=0\text{-}100\%FS) \qquad (2)$$

respectively. The molar ammonia flow ratio χ through the reactor, defined as the ratio of ammonia flow rate to total flow (precursor flow plus nitrogen), can be expressed in term of the percentage of full scale flow, z and y as

$$= \frac{0_{+\ 3}}{0_{total}} = \frac{0_{+\ 3}}{0_{Mai0_+2} + 0_{+\ 3}} = \frac{y}{50\ \ z + y}\ . \qquad (3)$$

where z represents the nitrogen main flow with 50 slm maximum flow (z= 0 to 100 %FS). The ammonia induced absorption has been characterized by UVAS in the wavelength range of 180 nm to 300 nm. Figure 3 shows the UV absorption spectra for ammonia flow ratios χ in the range of 10^{-1} to 10^{-3} at room temperature (RT) and a reactor pressure of 1.6 bar, which are typical molar ammonia flow ratios χ required for the growth of InN. As depicted in Figure 3, even for the lowest flow setting, several of the absorption structures at higher energies exhibit a saturation effect and are not suitable for ammonia characterization in the molar flow ratios. The absorption peak positions match those reported in literature[28,29] for a constant ammonia volume. No literature data were found for continuous ammonia flow characterization.

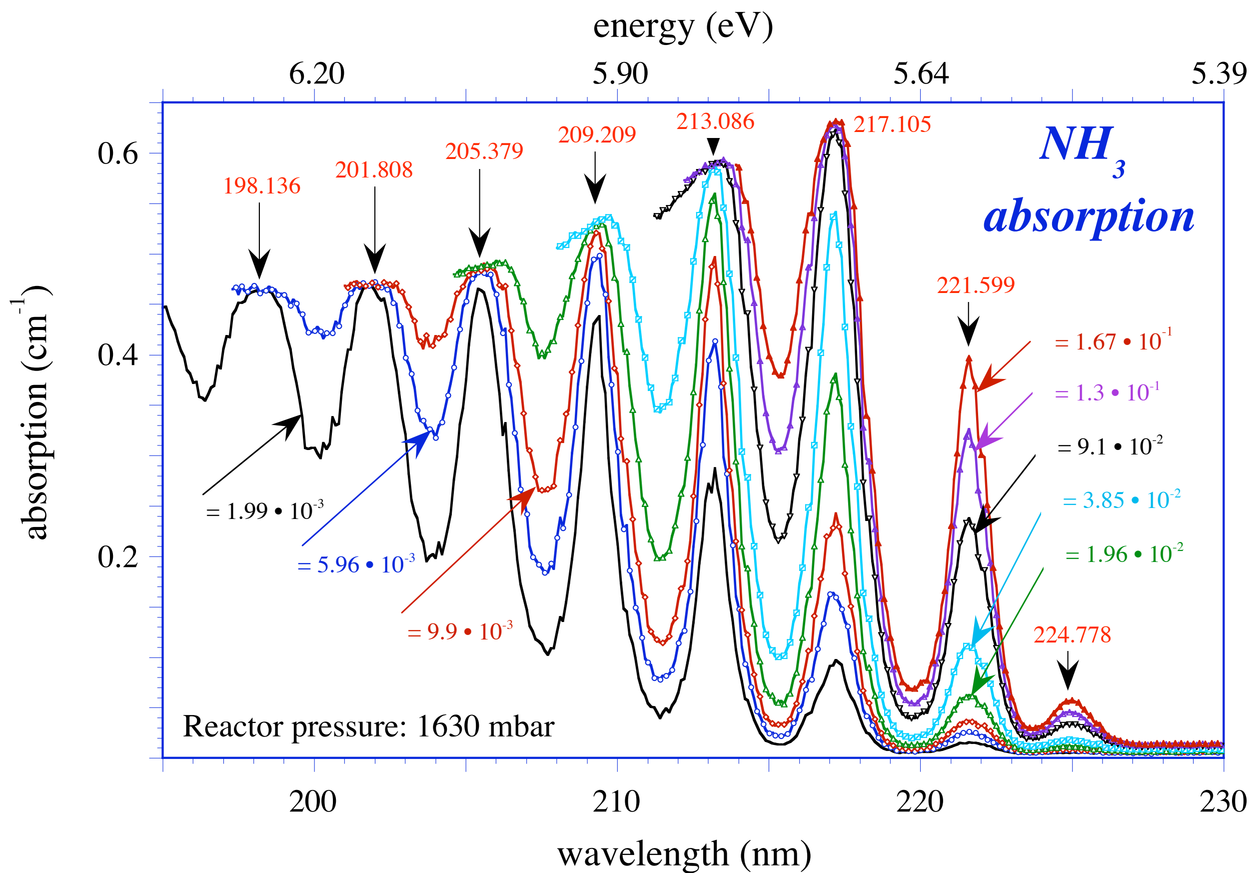

Figure 3: Absorption spectra for ammonia flow ratio χ in the range of 10^{-3} to 10^{-1} for a rector pressure of 1.6 bar.

In order to characterize ammonia molar flow rate below 10^{-3}, a second mass flow controller with 2 sccm full scale flow was utilized. The UV absorption spectra for ammonia flow ratios χ in the range of 10^{-4} to 10^{-5} are depicted in Figure 4. These spectra have been corrected in order to eliminate the nitrogen base line absorption. Overall, a total of 9 absorption features were identified being sensitive to molar ammonia flow rates less than a part per billion per sec. The

sensitivity ranges for each of the absorption peak maximum are summarized in table 1. The analysis of the peak maxima indicate a linear relationship between absorption peak maxima and the ammonia flow ratio in a double logarithmic scale[17].

For the growth of InN, ammonia flow ratios on the order of 10^{-2} are required. For these ammonia flow ratios, the UV absorption peaks at 217.1 nm and 221.6 nm are best suited for further analysis. However, due to the onset of saturation in the absorption peak at 217.1 nm, this peak will only be considered for ammonia flow ratios for smaller ammonia flows. The correlation for these two absorption peak maxima with the flow ratio χ can be expressed as

$$\begin{aligned} \alpha_{peak_217.1nn}(\chi) &= 0.38 \bullet \ln(\chi + 0.011) - 2.0 \bullet \chi + 1.73 \quad [\mathrm{cm}^{-1}] \\ \alpha_{peak_221.6nn}(\chi) &= -45 + 45.01 \bullet \exp\left(\chi/18\right) \bullet 10^{-2} \quad [\mathrm{cm}^{-1}] \end{aligned} \tag{4}$$

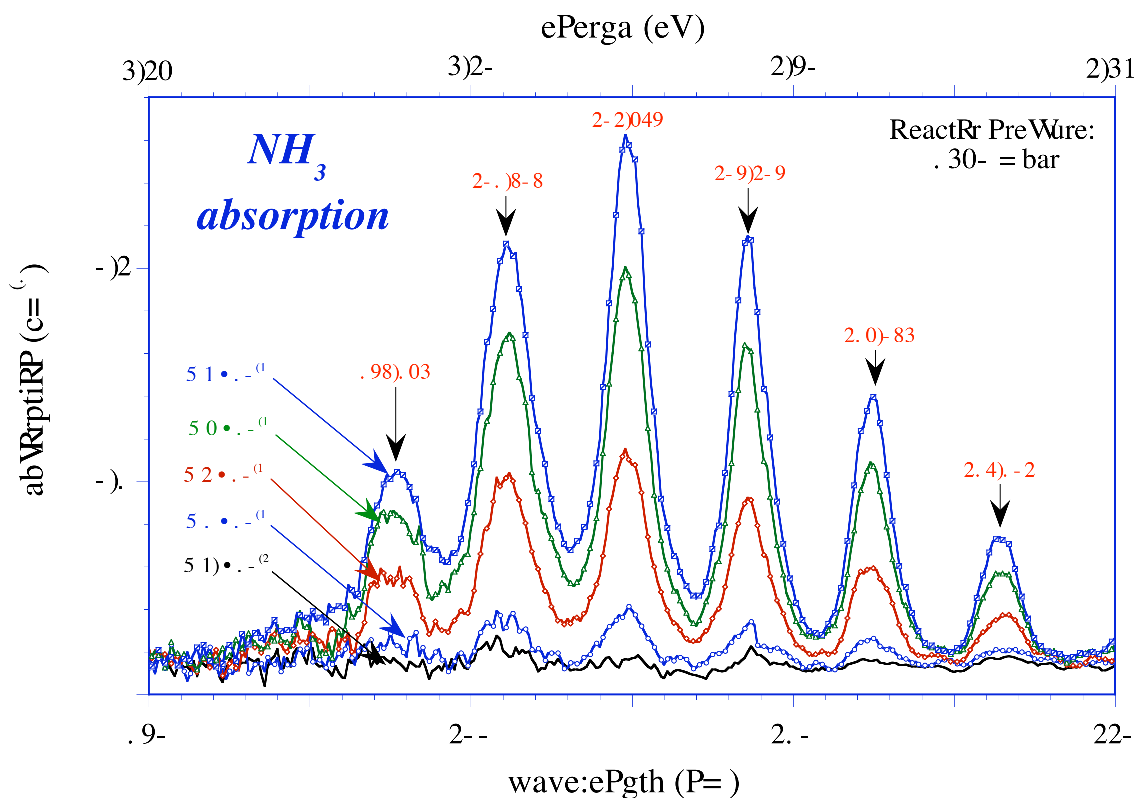

Figure 4: Absorption spectra for ammonia flow ratio χ in the range of 10^{-5} to 10^{-4} for a rector pressure of 1.6 bar.

Table 1: Ammonia absorption peak maxima and their sensitivity ranges

No.	Ammonia absorption peak maximum (nm)	Sensitivity range (Molecules per sec)
1	194.62	$< 10^{+15}$
2	198.136	$< 10^{+16}$
3	201.808	$< 10^{+16}$
4	205.378	$10^{+14} - 10^{+17}$
5	209.209	$10^{+15} - 10^{+17}$

6	213.086	$10^{+16} – 10^{+18}$
7	217.105	$10^{+17} – 10^{+19}$
8	221.599	$10^{+18} – 10^{+21}$
9	224.788	$10^{+21} – 10^{+23}$

For ammonia flow ratios in the range of $\chi = 1.0*10^{-2}$ to $1.6*10^{-1}$, the absorption maxima at 221.6 nm is used to provide the correlation between UV absorption and the molar flow ratio χ as shown in Figure 5a. The number of NH_3 molecules per unit time is computed as function of the observed UV absorption. For the UV absorption feature located at 221.6 nm, we find the number of NH_3 molecules per time unit as

$$N_{NH_3}(\lambda\text{=221.6nn}) = \frac{7.17 \bullet 10^{21} \bullet z \bullet \ln(\alpha')}{1 - 32 \bullet \ln(\alpha')} \quad [s^{-1}] \quad \text{with } \alpha' = \frac{\alpha_{@\ 221.6nn} - 80}{80.01}. \tag{5}$$

Figure 5b shows the correlation between ammonia moleculues per time unit and the ammonia flow ratio in the range of $\chi = 1.0 * 10^{-2}$ to $9.0 * 10^{-1}$, for a reactor pressure of 1.6 bar. Under those conditions, the ammonia flow varies between 10^{19} and $2.5*10^{20}$ NH_3 molecules per sec under continuous flow conditions.

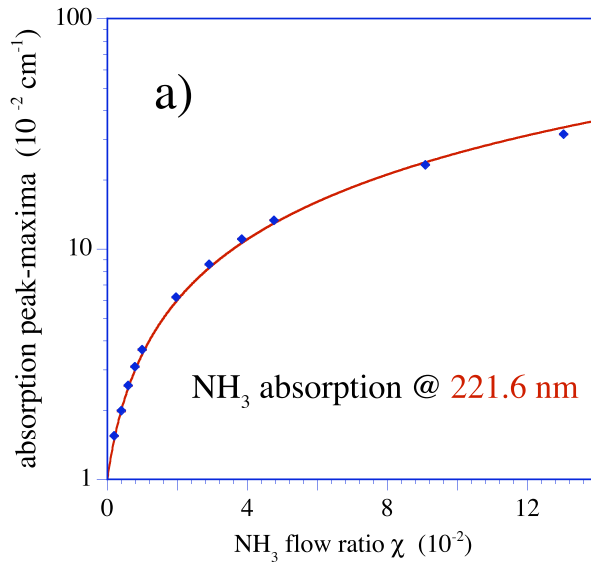

Figure 5a) Ammonia absorption monitored at λ = 221.6 nm as function of ammonia flow ratio χ under steady state flow conditions for a reactor pressure of 1.6 bar.

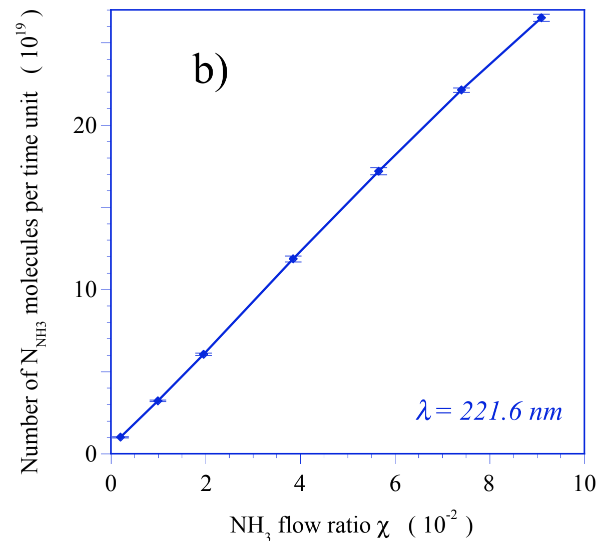

Figure 5b) Calculated concentration of ammonia molecules per sec using the absorption line at λ = 221.6 nm under continuous flow conditions.

III. UVAS characterization of pulsed ammonia injection

The flow of ammonia at higher pressures requires a compression and dilution step in order to allow ammonia gas to be injected in the HPCVD reactor. To accomplish this, an ammonia reservoir is filled at slightly above atmospheric pressure. In the following steps, the reservoir is

compressed with nitrogen carrier gas and temporally controlled injected into the reactor. The cycle repetition rate, duration of injection, and position of injection can the adjusted within 10 ms resolution. Figure 6 shows typical absorption traces for various ammonia flow rates monitored at 221.6 nm during pulsed ammonia injection with a 6 sec repetition period. The reactor pressure and total gas flow were kept constant. The total number of ammonia molecules flowing through the reactor can be calculated using the relationship between the UV absorption and ammonia flow rate provided by equation (5), taking in to account the compression ratio and gas reservoir volume.

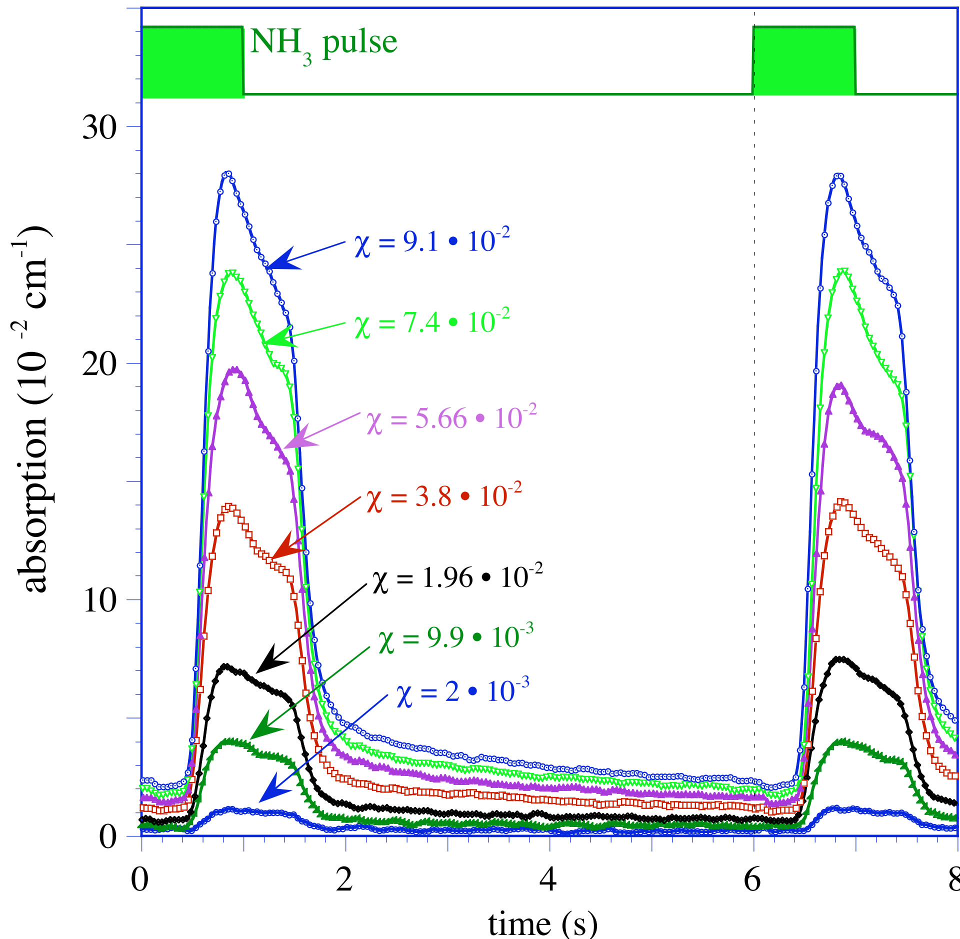

Figure 6

Ammonia absorption traces monitored at $\lambda = 221.6$ nm for 1 sec NH_3 pulses injected 6 sec apart.

The pulsed ammonia injection has been analyzed as function of pulse width, ammonia molecules per pulse, total reactor flow and reactor pressure. Figure 7 shows the monitored absorption traces at $\lambda = 221.6$ nm for various reactor pressures, while maintaining constant total gas flow at 5 slm and ammonia flow at 0.2 slm . A carryover of the UV absorption trace from one sequence to the next is observed at reactor pressures above 10 bar which results in an increase of the base line in the overall UV absorption.

As the reactor pressure is increased for a given fix flow rate, the ammonia pulses monitored at the substrate center line show three distinct features:

i) *a systematic shift in the pulse arrival time,*

ii) *a systematic ammonia pulse broadening, and*

iii) *a change in the NH_3 absorption cross section for pressures larger 8 bar.*

As shown in the following analysis, these distinct features provide crucial information pertaining to the reactor flow characteristics such as the average gas flow velocity. In addition, these features provide a pathway for the monitoring and engineering of the gas phase chemistry, which is crucial for the optimization of InN growth conditions. As shown in the following analysis, these distinct features provide crucial information pertaining to the reactor flow characteristics such as the average gas flow velocity. In addition, these features provide a pathway for the monitoring and engineering of the gas phase chemistry, which is crucial for the optimization of InN growth conditions.

Flow characterization during pulsed precursor injection:

The time delay Δt between the start of the ammonia pulse injection sequence and the arrival of the diluted ammonia gas to the center of the substrate is determined by the pneumatic valve opening time t_v, the reactor flow channel geometric factor r_g, the reactor pressure p_r (in bar) and the total gas flow through the reactor in terms of standard liters per min (slm) as:

$$\Delta t = t_v + \frac{l_d}{v_g} = t_v + r_g \cdot \frac{p_r}{V_{slm}} \qquad (6)$$

The reactor geometry factor r_g is a constant, containing parameters such as the reactor cross section A and the distance l_d between the injection valve and the substrate center line. Its unit is $[1 \cdot min^{-1} \cdot bar^{-1} \cdot s]$. The time differences Δt as analyzed for ammonia precursor pulse injection rates of 6 s is depicted in Figure 8 as function of total gas flow and reactor pressure. Analysis of the time delay under these conditions reveals that the pneumatic valve opening time t_v = 240 ms and the reactor geometry factor r_g = 0.70 can be treated as constant values.

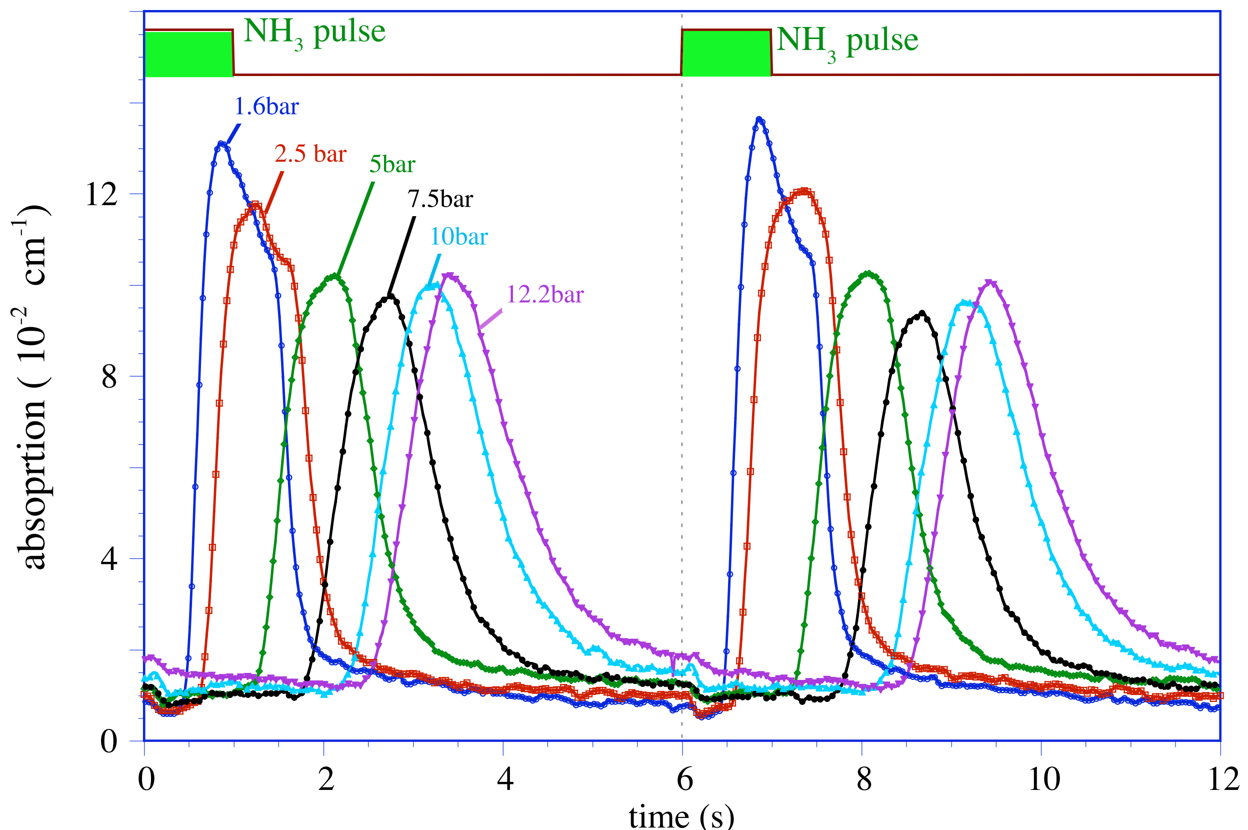

Figure 7: Absorption traces monitored at λ = 221.6 nm for 1 sec NH_3 pulses injected 6 s apart. The reactor main flow and the ammonia flow were kept constant at 5 slm nitrogen and 0.2 slm, respectively.

The analysis also provided corrected values for the actual total gas flow through the reactor, which deviates from the set flow for higher flow rates. Based on this analysis, the average gas flow velocity v_g through the reactor system can be computed as

$$v_g = \frac{1_{dr} \cdot V_{slm_{cor}}}{r_g \cdot p_r} = 136.7 \cdot \frac{V_{slm_{cor}}}{p_r}, \tag{7}$$

showing a direct relationship between the total gas flow V_{slm} and an inverse relationship to the reactor pressure. Note that this is the average gas flow velocity in the reactor system. Based on the reactor cross section and the gas volume per time unit, the average flow velocity over the substrate is estimated at a factor 2 smaller due to the larger reactor flow channel cross section as compared to the precursor and carrier gas lines.

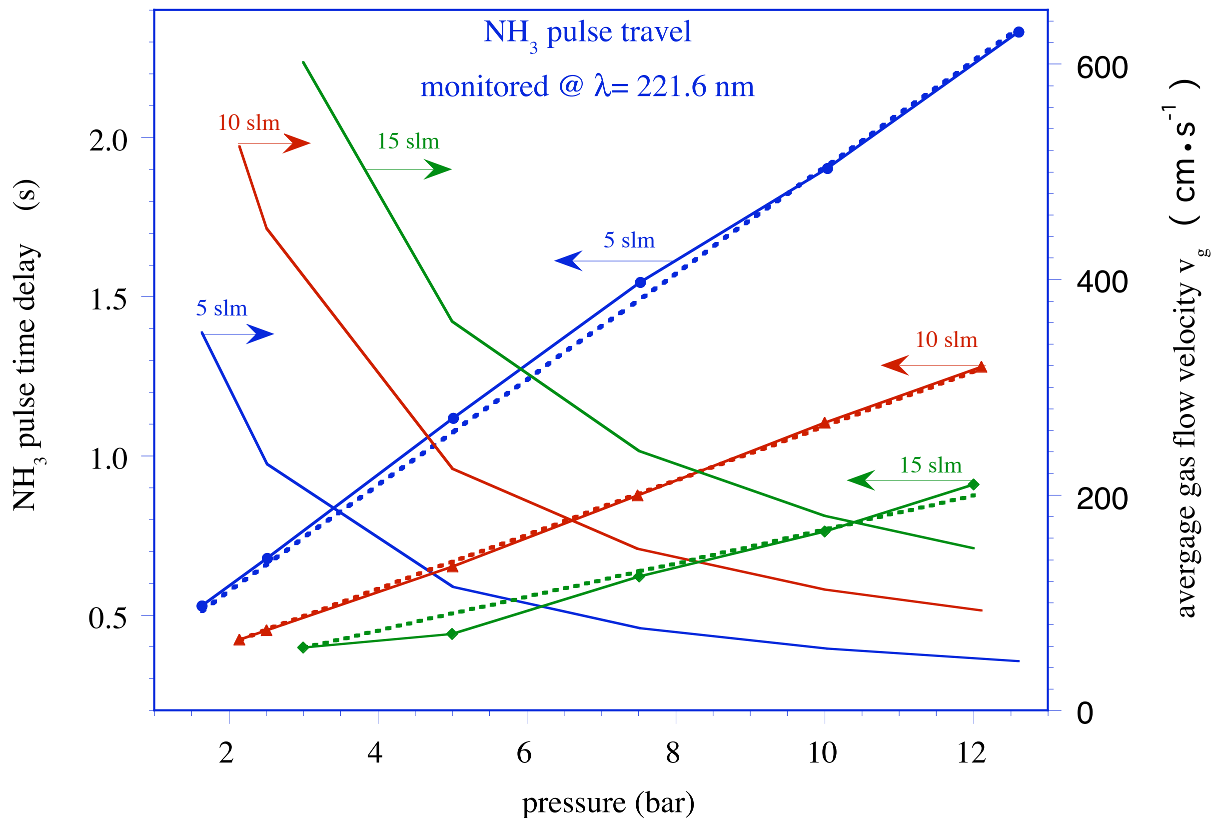

Figure 8: Time shift between injection and onset of pulse arrival at the substrate center line as function of the reactor pressure and for different flow rates. The right scale shows the computed average gas velocity v_g. between the ammonia reservoir and the substrate center line.

The systematic ammonia pulse broadening shown in Figure 7 can be directly explained from the relationship between gas flow velocity and pressure, as provided in equation 7. The reason for the pronounced increase in the NH_3 absorption observed for pressures larger than 8 bar is at present not fully understood and requires a more detailed study. However, one possible

explanation for this increase in the UV absorption is an increase in the UV absorption cross section for ammonia at elevated pressures. Such an increase in the UV absorption cross section would be beneficial for the decomposition kinetics of ammonia at elevated pressures as it would result in a more efficient decomposition of the ammonia precursor (see section V).

The pulsed precursor flow characterization allows for precise engineering of precursor pulse separation / overlap and with it the control of gas phase chemistry and surface chemistry during the growth process.

IV. Ammonia decomposition

The decomposition dynamics of ammonia have been analyzed in the temperature range of 300K to 1200K under continuous ammonia flow conditions for a reactor pressure of 1.6 bar. Figure 9 shows the change in the peak absorption maxima for an ammonia molar flow ratio χ of $4*10^{-3}$ as a function of temperature for absorption features found between 180 nm and 230 nm. The shift of the base line UV absorption due to the N_2 carrier gas has been taken in to account. As depicted in Figure 9, a significant reduction in the absorption strength is observed above 1000K, indicating the onset of decomposition of ammonia in the flow channel. The absorption peak maxima increase as the temperature rises due to the change in the absorption cross section. Above 900K a plateau is observed indicating the onset of decomposition with a strong cutoff above 1100K. Spectroscopic scans between 180 nm and 400 nm revealed no new UV absorption features (not shown here) that could be associated to ammonia fragments at elevated temperatures. However, a broad background absorption in the wavelength regime of 250 nm and 350 nm is observed for high temperatures, the origin of which is still under investigation.

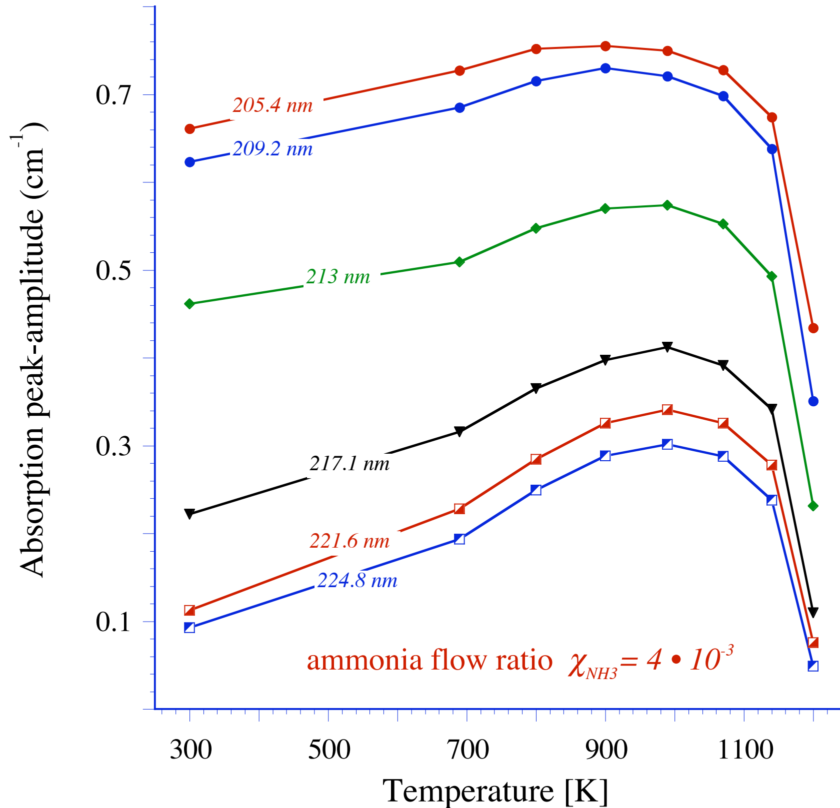

Figure 9
Ammonia absorption spectra taken at different temperatures during steady state flow conditions for a reactor pressure of 1.6 bar.

V. Ammonia and Trimethlyindium (TMI) decomposition at higher pressures

or the growth on InN, the decomposition dynamics of the precursors ammonia and TMI at higher pressures are of importance. Figure 10a shows the temperature dependency of the UV absorption of ammonia monitored at 210.7 nm while maintaining a reactor pressure of 10 bar. For this elevated pressure, the onset of decomposition as indicated by a decrease in the UV absorption occurs at a temperature of about 850K. This indicates a significant reduction in the decomposition temperature as compare to that at atmospheric pressure, where the onset of ammonia decomposition was observed at about 900 K (see Figure 9). As for ammonia, we also analyzed the TMI UV absorption spectrum, which has an absorption peak maximum at 213 nm. At present, there are no known experimental studies on the decomposition dynamics of TMI at higher pressures, however, several studies for low-pressure OMCVD growth conditions have been reported[23,30,31]. Figure 10b shows for comparison the TMI peak absorption as function of temperature, indicating that the onset of decomposition in the gas phase occurs around 800K. This onset in decomposition is slightly higher than those reported under low-pressure OMCVD conditions[23,30]. More detailed studies using UVAS and optical emission spectroscopy as function of pressure are required to correlate the experimental results to theoretical predications for the TMI decomposition at elevated pressures as formulated by Cardelino et al.[20].

The observed decrease of the temperature at which the onset of ammonia decomposition occurs under elevated pressure conditions is crucial for the optimization of the growth of InN and the control of point defect chemistry in this material system.

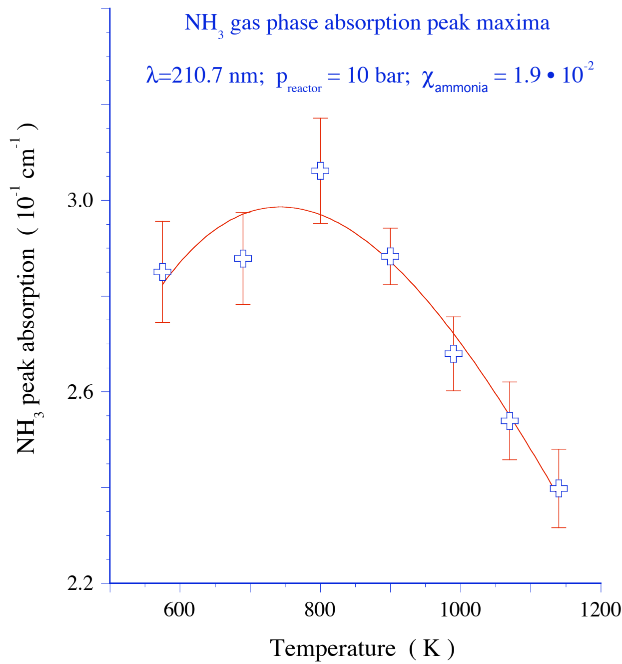

Figure 10a Change of the ammonia absorption peak maximum as function of temperature.

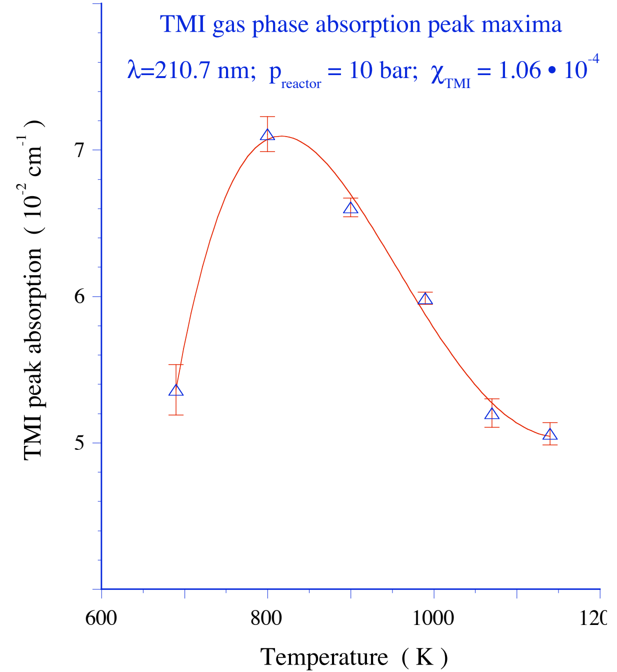

Figure 10b Decomposition of TMI at 10 bar reactor pressure, monitored during pulsed TMI injection as function of temperature.

VI. Conclusion

The flow kinetics and decomposition dynamics of the precursor gas ammonia have been studied by ultraviolet absorption spectroscopy (UVAS) during continuous flow and pulsed precursor injection. An analysis of the various UV absorption features with respect to the ammonia flow rates is provided, showing high sensitivity to less than a part per billion molecules per sec. For the ammonia molar flow ratios χ on the order of 10^{-2} to 10^{-1}, a direct relationship between the ammonia absorption strength at 221.6 nm and the ammonia flow rate is shown. Analysis of pulse shape and traveling time under a pulsed injection of ammonia yield the average gas flow velocity in the HPCVD system as function of the total gas flow rate and the reactor pressure. The onset of ammonia decomposition is found to start above 900K at atmospheric pressure. At higher reactor pressures, the onset of decomposition is shifted to lower temperature, indicating a better match to the decomposition kinetics of TMI for the growth of InN.

VII. Acknowledgments

We would like to acknowledge the support of this work by NASA grant NAG8-1686. M.S. gratefully acknowledges the fellowship of the Alexander von Humboldt-foundation.

VIII. References

1. T. Schmidtling, M. Drago, U. W. Pohl and W. Richter, J. Cryst. Growth **248** 523 (2003).
2. Bi Z.X. Bi, R. Zhang, Z.L. Xie, X.Q. Xiu, Y.D. Ye, B. Liu, S.L. Gu, B. Shen, Y. Shi and Y.D. Zheng, Mat. Lett. **58**(27-28) 3641 (2004).
3. J. Aderhold, V. Yu. Davydov, F. Fedler, H. Klausing, D. Mistele, T. Rotter, O. Semchinova, J. Stemmer and J. Graul, J. Cryst. Growth **222**(4) 701 (2001).
4. T. Tsuchiya, M. Ohnishi, A. Wakahara and A. Yoshida, J. Cryst. Growth **220**(3) 191 (2000).
5. V.Yu. Davydov, A.A. Klochikhin, V.V. Emtsev, D.A. Kurdyukov, S.V. Ivanov, V.A. Vekshin, F. Bechstedt, J. Furthmüller, J. Aderhold, J. Graul, A.V. Mudryi, H. Harima, A. Hashimoto, A. Yamamoto, E.E. Haller, Physica Status Solidi B, **234**(3) 787 (2002).
6. F.-H. Yang, J.-S. Hwang, K.-H. Chen, Y.-J.Yang, T.-H. Lee, L.-G. Hwa and L.-C. Chen, Thin Solid Films, **405**(1-2) 194 (2002).
7. V. Ya. Malakhov, Solar Energy Materials and Solar Cells, **76** 637 (2003).
8. A. G. Bhuiyan, A. Hashimoto, and A. Yamamoto, J. Appl. Phys. **94**(5) 2779 (2003).
9. V. Yu. Davydov, A. A. Klochikhin, V. V. Emtsev, A. V. Sakharov, S. V. Ivanov, V. A. Vekshin, F. Bechstedt, J. Furthmüller, J. Aderhold, J Graul, A. V. Mudryi, H. Harima, A. Hashimoto, A. Yamamoto, J. Wu, H. Feick and E. E. Haller, Proc. SPIE **5023** 68 (2003).
10. B. Onderka, J. Unland, R. Schmid-Fetzer, J. Mater. Res. **17** 3065 (2002).
11. J. MacChesney, P.M. Bridenbaugh, and P.B. O'Connor, Mater. Res. Bull. **5** 783 (1970).
12. O. Ambacher, M. S. Brandt, R. Dimitrov, T. Metzger, M. Stutzmann, R. A. Fischer, A. Miehr, A. Bergmajer, G. Dollinger; J. Vac. Sci. Technol. B **14** 3532 (1996).
13. N. Dietz, S. McCall, K.J. Bachmann, Proc. Microgravity Conf. 2000, NASA/CP-2001-210827 176 (2001).
14. N. Dietz, V. Woods, S. McCall and K.J. Bachmann, Proc. Microgravity Conf. 2002, NASA/CP-2003-212339 169 (2003).
15. N. Dietz, H. Born, M. Strassburg and V. Woods, Mat. Res. Soc. Symp. Proc. **798**, Y10.45.1 (2004).
16. V. Woods, H. Born, M. Strassburg and N. Dietz, J. Vac. Sci. Technol. A **22** 1596 (2004).
17. V. Woods and N. Dietz, Mat. Sci. Eng. B submitted (2004).
18. K.J. Bachmann, S. McCall, S. LeSure, N. Sukidi and F. Wang, J. Jpn. Soc. Microgravity Appl. Vol. **15** p. 436 (1998).
19. S. D. McCall and K. J. Bachmann, Mat. Res. Soc. Symp. Proc. Vol. **693**, I3.13.1 (2002).

[20] B. H. Cardelino, C. E. Moore, C. A. Cardelino, S. D. McCall, D. O. Frazier, K. J. Bachmann; J. Physical Chemistry A, **107** 3708 (2003).

[21] B. H. Cardelino, C. E. Moore, S. D. McCall, C. A. Cardelino, N. Dietz, K.J. Bachmann, CAITA-2004, Purdue University, June 2004, ISBN 86-7466-117-3 (2004).

[22] G. A. Hebner, K. P. Killeen and R. M. Biefeld, J. Cryst. Growth **98**(3) 293 (1989).

[23] G. A. Hebner and K. P. Killeen, J. Appl. Phys. **67** 1598 (1990).

[24] H. Okabe, M. K. Emadi-Babaki and V. R. McCrary, J. Appl. Phys. **69** 1730 (1991).

[25] M. C. Johnson, K. Poochinda, N. L. Ricker, J. W. Rogers Jr. and T. P. Pearsall, J. Cryst. Growth **212** 11 (2000).

[26] B. H. Cardelino, C. E. Moore, C. A. Cardelino, D. O. Frazier, K. J. Bachmann; J. Phys. Chem. A **105**(5), 849 (2001).

[27] N. Dietz, Mat. Sci. Eng. B **87**(1), pp.1 - 22 (2001)

[28] J. A. Syage, R. B. Cohen, and J. Steadman, J. Chem. Phys. **97** 6072 (1992).

[29] F. Z. Chen, D. L. Judge, C. Y. Robert Wu and John Caldwell, Planetary and Space Science **47**(1-2) 266 (1998)

[30] J. Haigh and S. O'Brien, J. Cryst. Growth **68** 550 (1984).

[31] R. J. S. J. A. McCaulley, and V. M. Donnelly, J. Vac. Sci. Technol. A **9** 2872 (1991).